LJMU Research Online

Verheul, J, Warmenhoven, J, Lisboa, P, Gregson, W, Vanrenterghem, J and Robinson, MA

 Identifying generalised segmental acceleration patterns that contribute to ground reaction force features across different running tasks

http://researchonline.ljmu.ac.uk/id/eprint/11063/

Article

1 **Identifying generalised segmental acceleration patterns that contribute to**

2 **ground reaction force features across different running tasks**

3

4 **Original research article**

5

6 **Authors**:

7 Jasper Verheul[1], John Warmenhoven[2,3], Paulo Lisboa[4], Warren Gregson[1], Jos Vanrenterghem[5], Mark

8 A. Robinson[1]

    1. Research Institute for Sport and Exercise Sciences, Liverpool John Moores University, Liverpool, United Kingdom

    2. Department of Exercise and Sports Science, The University of Sydney, Lidcombe, Australia

    3. Performance People & Teams, Australian Institute of Sport, Canberra, Australia

    4. Department of Applied Mathematics, Liverpool John Moores University, Liverpool, United Kingdom

    5. Department of Rehabilitation Sciences, KU Leuven, Leuven, Belgium

16

17 **Corresponding Author**:

18 Jasper Verheul (J.P.Verheul@ljmu.ac.uk)

19 Research Institute for Sport and Exercise Sciences, Liverpool John Moores University

20 Tom Reilly Building, Byrom Street, L3 5AF, Liverpool, United Kingdom

21

22 **Abstract word count**: 232

23 **Text-only word count**: 3041

24 **Number of figures and tables**: 2 figures and 1 table

25

26

1

27 **Abstract**

28 *Objective:* To support future developments of field-based biomechanical load monitoring tools, this

29 study aimed to identify generalised segmental acceleration patterns and their contribution to ground

30 reaction forces (GRFs) across different running tasks.

31 *Design*: Exploratory experimental design.

32 *Methods:* A multivariate principal component analysis (PCA) was applied to a combination of

33 segmental acceleration data from all body segments for fifteen team-sport athletes performing

34 accelerated, decelerated and constant low-, moderate- and high-speed running, and 90° cutting trials.

35 Segmental acceleration profiles were then reconstructed from each principal component (PC) and used

36 to calculate their specific GRF contributions.

37 *Results*: The first PC explained 48.57% of the acceleration variability for all body segments and was

38 primarily related to the between-task differences in the overall magnitude of the GRF impulse.

39 Magnitude and timing of high-frequency acceleration and GRF features (i.e. impact related

40 characteristics) were primarily explained by the second PC (12.43%) and also revealed important

41 between-task differences. The most important GRF characteristics were explained by the first five

42 PCs, while PCs beyond that primarily contained small contributions to the overall GRF impulse.

43 *Conclusions:* These findings show that a multivariate PCA approach can reveal generalised

44 acceleration patterns and specific segmental contributions to GRF features, but their relative

45 importance for different running activities are task dependent. Using segmental acceleration to assess

46 whole-body biomechanical loading generically across various movements may thus require task

47 identification algorithms and/or advanced sensor or data fusion approaches.

48 **Keywords**: Biomechanical loading; Principal component analysis; Segmental contributions; Running;

49 Accelerations

50

51 **Practical Implications**

52 • A multivariate PCA approach can be used to simultaneously identify general segmental

53 coordination patterns and specific segment contributions to GRF across running tasks, but

54 segment contributions to GRF vary between different movements.

55 • Caution should be practiced when using segmental acceleration signals to evaluate

56 biomechanical loads (e.g. from popular body-worn accelerometers), especially across different

57 tasks.

58 • Segmental acceleration information likely requires task identification algorithms and/or

59 advanced sensor or data fusion approaches to assess whole-body biomechanical loading

60 generically across various running movements.

61

Introduction

Although the physiological demands of sports have been monitored and investigated extensively in the field, biomechanical loads are still poorly quantified and not well understood [1]. Ground reaction forces (GRF) have, therefore, been suggested as a measure of external whole-body biomechanical loading, which might be estimated from currently popular body-worn accelerometers [2,3]. Estimating GRF from single accelerometers is, however, not straightforward [4–6]. Whilst there might be the potential of using full-body segmental accelerations to estimate GRF, reducing the number of segments to a number more feasible in a practical setting has been shown to substantially increase the GRF error [2,7]. These findings collectively suggest that estimating whole GRF waveforms accurately from segmental accelerations across different tasks is unlikely to be feasible. Since human running comprises a complex combination of simultaneous segmental movements however, more complex analyses may identify fundamental movement features that contribute to the GRF and could still be captured with accelerometers.

Principal component analysis (PCA) is a technique that can be used to reduce the amount of redundant information and extract key characteristics (e.g. magnitude, difference and phase shift operators [13,20]) of highly-dimensional biomechanical data. For example, PCA has been used to analyse gait patterns [8–10] and postural control [11,12], differentiate between pathological groups [10,13,14], or quantify and evaluate sports technique [15–17]. Although applications of PCA in biomechanics have typically focussed on waveform data for individual variables, multivariate PCA approaches allow for structures of variability to be uncovered across multiple parameters at the same time [8,9,15]. Given the complexity of segment coordination and interdependency of segmental accelerations during human running, a simultaneous analysis of multiple acceleration profiles is desirable to examine if generalised acceleration patterns across various segments exist and are related to specific GRF features. A multivariate PCA approach in which different variables (e.g. segments, tasks, time) are combined, might help to uncover such acceleration patterns and related GRF features across different running tasks, and reveal which specific segmental accelerations together influence changes in GRF profiles.

88   It is unlikely that GRF can be predicted from one or several segmental accelerations using mechanical

89   methods [3,4,6]. However, these approaches typically use acceleration signals from predefined segments

90   deemed important for GRF but do not allow for an agnostic identification of generalised multi-

91   segmental contributions to the GRF. We hypothesised that if explicit GRF features are related to

92   generalised acceleration patterns across different running tasks, this could further inform the potential

93   for using segmental accelerations to assess whole-body biomechanical loads in running-based sports

94   (such as the choice of relevant segments or the feasibility to generalise across tasks). Therefore, this

95   study aimed to use a multivariate PCA approach to identify segmental acceleration patterns that

96   contribute to GRF features, to more comprehensively understand biomechanical loading and support

97   future developments of field-based biomechanical load monitoring tools.

98   **Methods**

99   *Data*. A previously described data set of full-body kinematics and GRF data for right foot

100 contacts of fifteen healthy team-sport athletes (12 males and 3 females, age 23±4 years, height 178±9

101 cm, body mass 73±10 kg, sports participation 7±5 h per week) were used for this study [2]. This study

102 was approved by the Liverpool John Moores University ethics committee and participants provided

103 written informed consent according to the ethics regulations.

104 Participants performed accelerated, decelerated, low- (2-3 m·s^{-1}) moderate- (4-5 m·s^{-1}) and high-speed

105 (>6 m·s^{-1} including maximal sprinting) running, and 90° cutting [2]. Seventy-six marker trajectories

106 were measured from a three-dimensional motion capture system (Qualisys Inc., Gothenburg, Sweden),

107 while GRFs were measured from a force platform (Kistler Holding AG, Winterthur, Switzerland).

108 Kinematic and kinetic data were exported to Visual3D (C-motion, Germantown, MD, USA), which

109 was used to build a fifteen segment (head, trunk, pelvis, upper arms, forearms, hands, thighs, shanks

110 and feet) six-degree-of-freedom model [2]. Centre of mass (CoM) accelerations for each segment were

111 calculated as the double differentiation of segmental CoM positions.

112 *Normalisation and scaling*. All fifteen segmental CoM acceleration and GRF waveforms in

113 the mediolateral (x), anteroposterior (y) and vertical (z) direction during ground contact were

114 normalised to 101 data points for each trial. Segmental accelerations were then expressed as

115 acceleration vectors **a** for every time point t (equation 1) (note: vectors and matrices will be referred to

116 by using bold lowercase or capital letters respectively).

$$\mathbf{a}(t) = [ax_1(t), ay_1(t), az_1(t), ax_2(t), \ldots, az_{15}(t)] \qquad \text{Eq.1}$$

117 The combination of acceleration vectors for each trial thus formed a 101×45 acceleration matrix $\mathbf{A^{trial}}$.

118 Trial-specific acceleration matrices were then combined in participant- and task-specific matrices

119 $\mathbf{A^{part,task}}$ by vertically stacking each trial matrix $\mathbf{A^{trial}}$ per participant and task. These combined

120 acceleration matrices $\mathbf{A^{part,task}}$ were normalised and scaled to 1) assure that every participant equally

121 contributed to the variance of the total acceleration matrix, 2) reduce anthropometric differences

122 between participants, 3) preserve relative segmental acceleration amplitudes and 4) correctly represent

123 the portion of the total body mass of each segment [12]. First, a participant- and task-specific mean

124 acceleration vector $\overline{\mathbf{a}^{part,task}}$ was calculated and subtracted from each acceleration vector **a** (equation

125 2), to assure that the first PC described the direction of maximum variance in the segmental

126 acceleration data.

$$\mathbf{A^{part,task\prime}}(t) = \left[\left(ax_1(t) - \overline{ax_1^{part,task}}\right), \left(ay_1(t) - \overline{ay_1^{part,task}}\right), \ldots, \left(az_{15}(t) \right. \right.$$
$$\left. \left. - \overline{az_{15}^{part,task}}\right)\right] \qquad \text{Eq.2}$$

127 Matrix $\mathbf{A^{subj,task\prime}}$ thus represented the acceleration deviations from the participant's mean segmental

128 acceleration for each task. Secondly, acceleration vectors for each participant were divided by the

129 mean Euclidean norm $\overline{\mathbf{euc_{norm}}^{part,task}}$ of all acceleration vectors (equation 3), to ensure that

130 participants equally contributed to the variance of the total acceleration matrix and to minimise

131 amplitude differences due to anthropometric differences [11,18].

$$\mathbf{A^{part,task\prime\prime}}(t) = \frac{\mathbf{A^{part,task\prime}}(t)}{\mathbf{euc_{norm}^{part,task}}} \qquad \text{Eq.3}$$

132 Thirdly, each acceleration vector was normalised for the relative segmental masses to further account

133 for anthropometric differences between segments. Acceleration vectors were multiplied by a weight

134 vector **w** (equation 4), which contained mass ratios of each segment relative to the total body mass [19].

$$A^{part,task'''}(t) = w \cdot A^{part,task''}(t) \qquad \text{Eq.4}$$

135   Finally, the participant- and task-specific acceleration matrices for each participant $A^{part,task'''}$ were

136   combined in one 48783×45 (15 participants · 6 tasks · number of trials per task (483 in total) · 101

137   data points per trial) acceleration matrix A.

138   *Principal component analysis*. A PCA was performed on the normalised and combined

139   acceleration matrix A. The results included 1) eigenvector matrix EV consisting of 45 orthogonal

140   eigenvectors ev_k, (or 'principal component vectors') each indicating the largest acceleration variability

141   for all segments, 2) eigenvalue matrix λ containing the eigenvalues λ_k which quantified the amount of

142   variability described by each eigenvector ev_k, with a strict decrease in the amount of variability with

143   increasing k, and 3) time evolution coefficient matrix C (or 'score matrix') describing how the original

144   segmental acceleration data evolved along the new principal acceleration axes. C was calculated by

145   projecting each original normalised and scaled acceleration vector a onto each PC_k of the eigenvector

146   matrix [12], according to equation 5.

$$c_k(t) = a(t) \cdot ev_k \qquad \text{Eq.5}$$

147   *Principal accelerations and principal GRF*. Participant- and task-specific principal

148   acceleration (PA) matrices $PA^{part,task}$ were reconstructed for each individual PC_k (equation 6) to

149   investigate how patterns of acceleration contribute to the GRF, or the sum of the first k PCs (equation

150   7) to examine the number of PCs required to adequately describe the whole GRF waveform. PCs were

151   expressed in the original segmental acceleration space by decomposing reconstructed acceleration

152   matrices into participant- and task-specific matrices, after which the normalisation and scaling steps

153   were retraced.

$$PA_k^{part,task}(t) = \overline{a^{part,task}} + \overline{euc_{norm}^{part,task}} \cdot w^{-1} \cdot [C_k \cdot ev_k]^{part,task} \qquad \text{Eq.6}$$

$$PA_{1-k}^{part,task}(t) = \overline{a^{part,task}} + \overline{euc_{norm}^{part,task}} \cdot w^{-1} \cdot \left[\sum_{k=1}^{1,2,\dots,45} C_k \cdot ev_k \right]^{part,task} \qquad \text{Eq.7}$$

154   Since the reconstructed PAs are consistent with the laws of Newtonian mechanics, the principal

155   segmental acceleration vectors pa can be used to calculate principal GRF (PGRF) profiles. PGRF was

156   defined as the part of the overall GRF that is associated with the totality of all segment PAs combined.

157   Resultant PGRF curves were calculated as the sum of the product of each segmental mass and

158   principal CoM acceleration in the three directions, from each individual PC_k (equation 8), or from the

159   sum of PAs reconstructed from the first k PCs (equation 9; Fig. 1).

$$\mathbf{PGRF_k} = \sqrt{\left(\sum_{n=1}^{15}(\mathbf{pa_{k,n,x}} \cdot m_n)\right)^2 + \left(\sum_{n=1}^{15}(\mathbf{pa_{k,n,y}} \cdot m_n)\right)^2 + \left(\sum_{n=1}^{15}(\mathbf{pa_{k,n,z}} \cdot m_n) + g \cdot BM\right)^2} \qquad \text{Eq. 8}$$

$$\sum \mathbf{PGRF_{1-k}} = \sum_{pc=1}^{k}\left[\sqrt{\left(\sum_{n=1}^{15}(\mathbf{pa_{k,n,x}} \cdot m_n)\right)^2 + \left(\sum_{n=1}^{15}(\mathbf{pa_{k,n,y}} \cdot m_n)\right)^2 + \left(\sum_{n=1}^{15}(\mathbf{pa_{k,n,z}} \cdot m_n) + g \cdot BM\right)^2}\right] \qquad \text{Eq. 9}$$

160   In which k is the PC number, **pa** the principal segmental acceleration in x, y or z direction, m the

161   segmental mass, n the number of segments (n=15), g the gravitational acceleration (-9.81 $m \cdot s^{-1}$) and

162   BM the total body mass. Measured and calculated PGRF curves were normalised to each participant's

163   body mass and accuracy evaluated as the curve root mean squared error (RMSE) relative to the

164   measured GRF.

165   **Results**

166   Visual screening of PC results revealed that distinct acceleration and GRF features were primarily

167   explained by the first five PCs, which explained 77.8% of all segmental acceleration variability across

168   participants and tasks. Each additional PC (i.e. k>5) explained <3% variance of the original

169   acceleration data and contributed <1% to the overall GRF. Therefore, only the first five PGRF and

170   ∑PGRF profiles (see Fig. 1 for an example), and associated PAs were used for further qualitative

171   analysis.

172   PC_1 explained 48.6% of the acceleration variability of all segments, which accounted for the majority

173   of the overall GRF impulse (Fig. 2; Table 1). The largest amplitude of PA_1 occurred between ~10-70%

174   of stance (Fig. A.1 and A.2) for decelerated and constant-speed running, but later during stance (~30-

175   90%) for accelerated running. PA_1 magnitudes were typically the lowest for 90° cutting and running at

176   slower speeds and the highest for the forearms and hands.

177 Including PC_2 reduced $\sum PGRF$ errors by 25.5% across tasks (Table 1). PC_2 primarily explained high-

178 frequency acceleration contributions to the GRF impact peak associated with landing (Fig. 2), for all

179 tasks except accelerations, and were primarily expressed in PA_2 profiles of the right thigh, shank and

180 foot (stance leg segments) and pelvis. In contrast to the other tasks, $PGRF_2$ features for accelerated

181 running occurred during the second half of stance (i.e. ~50-90%).

182 Segmental accelerations from PC_3 were associated with two GRF features for constant-speed running,

183 but not for the other tasks. $PGRF_3$ contained small impact peak force components during early stance

184 (~20-30%), as well as a general contribution to GRF impulse during the second half of stance (Fig. 2).

185 Magnitudes for both GRF features increased with running speed and were primarily associated with

186 accelerations of leg and arm segments (Fig. A.2).

187 Compared to the first three PCs, PC_4 and PC_5 contained considerably less segmental acceleration

188 variability and distinct GRF features (Table 1). For accelerated running, these PCs made constant (but

189 small) GRF contributions from ~10-80% ($PGRF_4$) and ~0-50% ($PGRF_5$) of stance (Fig. 2), while for

190 other movements, PA_4 profiles were mainly associated with small GRF contributions during the first

191 ~40% of stance. For high-speed running, $PGRF_5$ contained a considerable amount of GRF impulse,

192 but not for the other tasks.

193 Including more PCs (i.e. k>5) gradually increased the overall GRF and reduced $\sum PGRF$ errors but

194 were not related to specific GRF features. To achieve $\sum PGRF$ errors within 10% of the mean RMSE

195 for GRF from all 45 PCs (i.e. the original data), a total of 18 (accelerations), 2 (decelerations), 15 (90°

196 cuts), 7 (low-speed running), 4 (moderate-speed running) and 18 (high-speed running) PCs were

197 required, respectively.

Discussion

199   *Task-specific accelerations*. The aim of this study was to identify key contributions of

200 generalised acceleration patterns and specific segments to the GRF. The three primary modes of

201 variation described by PCA; a magnitude operator, difference operator and phase shift [13,20], were

202 evident in the first five PAs and PGRFs. First, segmental acceleration magnitude differences

203   associated with GRF impulse (i.e. overall loading of the body) and the impact peak were captured by

204   PC_1 and PC_2 respectively. Substantial amplitude variability in PA and PGRF profiles between tasks

205   showed that the magnitude of these GRF characteristics was strongly dependent on task (Fig. 2).

206   Secondly, PC_3 and PC_5 highlighted difference operator features. For accelerated running for example,

207   the main contributions of $PGRF_3$ and $PGRF_5$ to the overall GRF was during the first half of stance but

208   explained a much lower amount of force during push-off, while for constant-speed running this was

209   the other way around. Thirdly, clear phase shift characteristics were manifested in the first two PCs.

210   For example, the impulse peak ($PGRF_1$) and high-frequency acceleration and force features of PC_2

211   appeared in the first ~10-40% of stance for decelerations, constant-speed running and cutting tasks,

212   but much later during stance for accelerated running. These results show that PCA can identify general

213   acceleration patterns underlying specific GRF profiles, as well as highlight the relative importance of

214   these features for different running tasks.

215   PC_2 primarily contained acceleration and force features related to the GRF impact peak, for all tasks

216   except accelerations. These force peaks were mostly explained by high PA_2 peaks of the support leg's

217   foot, shank and thigh segment, and the pelvis to a lesser extent (Fig. A.1 and A.2). This supports

218   previous suggestions that the impact peak is primarily associated with stance leg accelerations [21–23].

219   Moreover, despite the absence of visual impact peaks in GRF waveforms for non-rearfoot running

220   gaits (e.g. sprinting), force frequencies associated with these initial force peaks are still present [24,25].

221   Clear impact force peaks were indeed found in $PGRF_2$ profiles for high-speed running, for which

222   runners typically switched to a forefoot landing technique (Fig. 2). The present PCA approach thus

223   further supports the presence of impact force peaks in non-rearfoot running, despite their visual

224   absence in the GRF waveform.

225   For accelerated running, PA_2 profiles of the support leg's foot, shank and thigh segments were mainly

226   related to a force peak during the second half of stance (Fig. 2). In addition, the smoother impacts of

227   landing during accelerations were better explained by PC_5 and thus less important for the overall

228   biomechanical load on the body. This highlights the importance of force production when pushing off

229   the ground in acceleration movements, compared to other tasks in which braking (force) is emphasised

230   more. Using PCA across multiple tasks can thus not only identify generic acceleration patterns, but

231   also explain their relative importance for different running movements.

232   The results of this study highlight that segment contributions to GRF are movement dependent. These

233   findings could explain why generalised methods to predict GRF from one or a few acceleration signals

234   cannot lead to accurate GRF estimates across different tasks [2,7]. For example, a specific segment (or

235   combination of segments) might be suitable to estimate GRF profiles for sprinting, while the same

236   segments are not so suitable to describe the GRF for decelerated running. Therefore, one should be

237   cautious when using generic biomechanical models or approaches to estimate GRF and/or assess

238   external biomechanical loads from segmental accelerations across different running tasks.

239   *Segment-specific accelerations.* Trunk accelerometry is arguably the most commonly used

240   acceleration signal for assessing biomechanical loads in different sports [26–28]. Although the trunk is

241   thought to be the main contributor to GRF [21], trunk PA_1 profiles were very similar to other segments,

242   for all tasks (Fig. A.1 and A.2). Moreover, higher PCs (i.e. k>1) did not explain any considerable

243   additional trunk acceleration features. These findings thus suggest that the trunk's large contributions

244   to GRF are primarily due to its large mass rather than the characteristics of its acceleration. The value

245   of using trunk accelerometry alone for biomechanical load monitoring purposes is thus probably

246   limited.

247   PAs of the forearm and hand segments typically had a high magnitude of acceleration (Fig. A.1 and

248   A.2) but did not make any distinct contribution to the specific GRF features in the first five PCs.

249   Furthermore, for decelerated and low- to moderate-speed running considerably less PCs were required

250   to achieve $\sum$PGRF errors within 10% of the mean RMSEs from all 45 PCs. This is possibly caused by

251   the more profound and complex arm movements (explained by PCs beyond the first five) during

252   acceleration, cutting and sprinting movements. Therefore, although arm movements (but also swing

253   leg motion) are not the primary contributors to GRF, these segments do account for a considerable part

254   of overall GRF impulse. These findings highlight that all segments should be considered when

255   assessing whole-body loading, especially for sports in which dynamic and high-intensity tasks are

256   frequently performed.

11

257   It should be acknowledged that directly measuring PAs (e.g. from multiple body-worn accelerometers)

258   may not be feasible in training and competition environments, making it difficult to translate the

259   present findings to a field-based load monitoring context. The multivariate PCA approach used in this

260   study could, however, uncover a deeper layer of complexity and highlight key characteristics in a

261   high-dimensional acceleration data set. This complexity adds to previous findings that reconstructing

262   GRF waveforms from less than all segments across different tasks is unlikely feasible [2]. The PCA

263   allowed for different acceleration combinations and key features to be detected, which provides

264   practical insight for what sensors to include when using too many sensors is an issue in the field.

265   Regardless, the complexity of segmental contributions to GRF outlined in this study further

266   emphasises that estimating biomechanical loading from accelerations is not straightforward, especially

267   across different tasks. Therefore, using body-worn accelerometry to estimate whole-body

268   biomechanical loading across various movements likely requires task identification algorithms and/or

269   advanced sensor or data fusion approaches (e.g.[29]).

270   *Limitations*. The methods described in this study have several limitations. First, PCA was

271   deliberately performed on the combined segmental accelerations for multiple participants and tasks.

272   The results are thus a general representation of how segmental acceleration contribute to GRF, across

273   different running tasks. Unique loading or movement features for individual athletes or tasks may thus

274   not be highlighted and future research could consider task- and/or participant-specific PCA. Secondly,

275   using resultant accelerations and GRFs did not allow for identifying direction-specific acceleration and

276   GRF features. However, this study aimed to evaluate generic acceleration patterns related to overall

277   biomechanical load features. Moreover, body-worn accelerometers cannot typically distinguish

278   between global x-y-z directions and using resultant accelerations was deemed more feasible for

279   potential translations of our findings to a field-based load monitoring context. Thirdly, segmental

280   acceleration data were normalised by a weighting vector based on a standardised mass distribution [19].

281   Due to typical anthropometric differences between participants, defining and applying an

282   individualised mass distribution could affect the results. Although this was beyond the scope of this

283   study, future work could consider if personalised normalisation may be beneficial.

284 **Conclusions**

285 This study aimed to identify general segmental acceleration patterns associated with GRF features that

286 might be used to assess whole-body biomechanical loads. Although a multivariate PCA could reveal

287 generic acceleration patterns and specific segmental contributions to GRF, the relative importance of

288 these features varied between tasks. Using segmental acceleration to assess whole-body biomechanical

289 loading generically across different movements thus likely requires task identification algorithms

290 and/or advanced sensor or data fusion approaches.

293 **Supplementary files**

294 Fig. A.1 and A.2 can be found in Appendix A, which is available as an online supplementary

295 document.

References

297   1.   Vanrenterghem J, Nedergaard NJ, Robinson MA, Drust B. Training Load Monitoring in Team

298   Sports: A Novel Framework Separating Physiological and Biomechanical Load-Adaptation

299   Pathways. *Sport Med*. 2017;47(11):2135-2142. doi:10.1007/s40279-017-0714-2

300   2.   Verheul J, Gregson W, Lisboa PJ, Vanrenterghem J, Robinson MA. Whole-body

301   biomechanical load in running-based sports: The validity of estimating ground reaction forces

302   from segmental accelerations. *J Sci Med Sport*. 2019;22(6):716-722.

303   doi:10.1016/j.jsams.2018.12.007

304   3.   Nedergaard NJ, Robinson MA, Eusterwiemann E, Drust B, Lisboa PJ, Vanrenterghem J. The

305   Relationship Between Whole-Body External Loading and Body-Worn Accelerometry During

306   Team-Sport Movements. *Int J Sports Physiol Perform*. 2017;12(1):18-26.

307   https://search.ebscohost.com/login.aspx?direct=true&db=sph&AN=121191349&site=ehost-

308   live.

309   4.   Nedergaard NJ, Verheul J, Drust B, et al. The feasibility of predicting ground reaction forces

310   during running from a trunk accelerometry driven mass-spring-damper model. *PeerJ*.

311   2018;6:e6105. doi:10.7717/peerj.6105

312   5.   Raper DP, Witchalls J, Philips EJ, Knight E, Drew MK, Waddington G. Use of a tibial

313   accelerometer to measure ground reaction force in running: A reliability and validity

314   comparison with force plates. *J Sci Med Sport*. 2018;21(1):84-88.

315   doi:10.1016/j.jsams.2017.06.010

316   6.   Edwards S, White S, Humphreys S, Robergs R, O'Dwyer N. Caution using data from triaxial

317   accelerometers housed in player tracking units during running. *J Sports Sci*. 2018:1-9.

318   doi:10.1080/02640414.2018.1527675

319   7.   Pavei G, Seminati E, Cazzola D, Minetti AE. On the estimation accuracy of the 3D body center

320   of mass trajectory during human locomotion: Inverse vs. forward dynamics. *Front Physiol*.

321   2017;8(129):1-13. doi:10.3389/fphys.2017.00129

322 8. Daffertshofer A, Lamoth CJCC, Meijer OG, Beek PJ. PCA in studying coordination and

323   variability: A tutorial. *Clin Biomech*. 2004;19(4):415-428.

324   doi:10.1016/j.clinbiomech.2004.01.005

325 9. Troje NF. Decomposing biological motion: A framework for analysis and synthesis of human

326   gait patterns. *J Vis*. 2002;2:371-387. http://journalofvision.org/2/5/2/.

327 10. Federolf PA, Boyer KA, Andriacchi TP. Application of principal component analysis in

328   clinical gait research: Identification of systematic differences between healthy and medial

329   knee-osteoarthritic gait. *J Biomech*. 2013;46(13):2173-2178.

330   doi:10.1016/j.jbiomech.2013.06.032

331 11. Federolf PA, Roos L, Nigg BM. Analysis of the multi-segmental postural movement strategies

332   utilized in bipedal, tandem and one-leg stance as quantified by a principal component

333   decomposition of marker coordinates. *J Biomech*. 2013;46:2626-2633.

334   doi:10.1016/j.jbiomech.2013.08.008

335 12. Federolf PA. A novel approach to study human posture control: "Principal movements"

336   obtained from a principal component analysis of kinematic marker data. *J Biomech*.

337   2016;49:364-370. doi:10.1016/j.jbiomech.2015.12.030
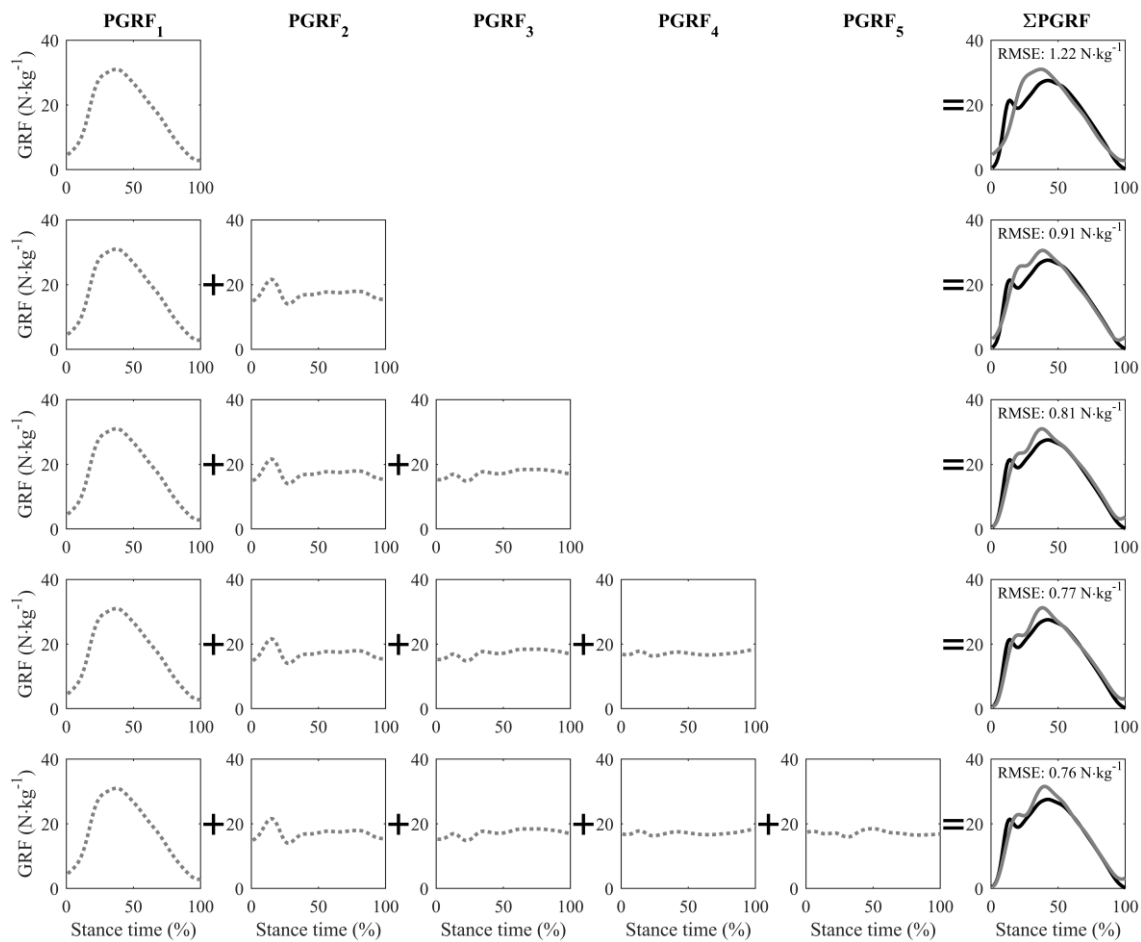
338 13. Wrigley AT, Albert WJ, Deluzio KJ, Stevenson JM. Differentiating lifting technique between

339   those who develop low back pain and those who do not. *Clin Biomech*. 2005;20:254-263.

340   doi:10.1016/j.clinbiomech.2004.11.008

341 14. Deluzio KJ, Wyss UP, Zee B, Costigan PA, Sorbie C. Principal component models of knee

342   kinematics and kinetics: Normal vs. pathological gait patterns. *Hum Mov Sci*. 1997;16:201-217.

343   doi:10.1016/S0167-9457(96)00051-6

344   15.   Federolf PA, Reid R, Gilgien M, Haugen P, Smith G. The application of principal component

345   analysis to quantify technique in sports. *Scand J Med Sci Sports*. 2014;24:491-499.

346   doi:10.1111/j.1600-0838.2012.01455.x

347   16.   Boyer KA, Silvernail JF, Hamill J. The Role of Running Mileage on Coordination Patterns in

348   Running. *J Appl Biomech*. 2014;30:649-654. doi:10.1123/JAB.2013-0261

349   17.   Warmenhoven J, Cobley S, Draper C, Harrison A, Bargary N, Smith R. How gender and boat-

350   side affect shape characteristics of force – angle profiles in single sculling: Insights from

351   functional data analysis. *J Sci Med Sport*. 2018;21(5):533-537.

352   doi:10.1016/j.jsams.2017.08.010

353   18.   Gløersen Ø, Myklebust H, Hallén J, Federolf PA. Technique analysis in elite athletes using

354   principal component analysis. *J Sports Sci*. 2018;36(2):229-237.

355   doi:10.1080/02640414.2017.1298826

356   19.   Dempster WT. Space requirements of the seated operator: Geometrical, Kinematic, and

357   Mechanical Aspects of the Body With Special Reference to the Limbs. *WADC Tech Rep*.

358   1955:55-159.

359   20.   Brandon SCE, Graham RB, Almosnino S, Sadler EM, Stevenson JM, Deluzio KJ. Interpreting

360   principal components in biomechanics: Representative extremes and single component

361   reconstruction. *J Electromyogr Kinesiol*. 2013;23:1304-1310.

362   doi:10.1016/j.jelekin.2013.09.010

363   21.   Bobbert MF, Schamhardt HC, Nigg BM. Calculation of vertical ground reaction force

364   estimates during running from positional data. *J Biomech*. 1991;24(12):1095-1105.

365   doi:10.1016/0021-9290(91)90002-5

366   22.   Shorten M, Mientjes MIV. The "heel impact" force peak during running is neither "heel" nor

367   "impact" and does not quantify shoe cushioning effects. *Footwear Sci*. 2011;3(1):41-58.

368   doi:10.1080/19424280.2010.542186

369   23.   Clark KP, Ryan LJ, Weyand PG. A general relationship links gait mechanics and running

370   ground reaction forces. *J Exp Biol*. 2017;220(2):247-258. doi:10.1242/jeb.138057

371   24.   Hamill J, Gruber AH. Is changing footstrike pattern beneficial to runners? *J Sport Heal Sci*.

372   2017;6:146-153. doi:10.1016/j.jshs.2017.02.004

373   25.   Gruber AH, Edwards WB, Hamill J, Derrick TR, Boyer KA. A comparison of the ground

374   reaction force frequency content during rearfoot and non-rearfoot running patterns. *Gait*

375   *Posture*. 2017. doi:10.1016/j.gaitpost.2017.04.037

376   26.   Colby MJ, Dawson B, Heasman J, Rogalski B, Gabbett TJ. Accelerometer and GPS-Derived

377   Running Loads and Injury Risk in Elite Australian Footballers. *J Strength Cond Res*.

378   2014;28(8):2244-2252.

379   27.   Akenhead R, Marques JB, Paul DJ. Accelerometer load: a new way to measure fatigue during

380   repeated sprint training? *Sci Med Footb*. 2017;1(2):151-156.

381   doi:10.1080/24733938.2017.1330550

382   28.   Buchheit M, Gray A, Morin J-B. Assessing stride variables and vertical stiffness with GPS-

383   embedded accelerometers: preliminary insights for the monitoring of neuromuscular fatigue on

384   the field. *J Sport Sci Med*. 2015;(14):698-701.

385   29.   Johnson WR, Mian A, Robinson MA, Verheul J, Lloyd DG, Alderson JA. Multidimensional

386   ground reaction forces and moments from wearable sensor accelerations via deep learning.

387   *arXiv Prepr*. 2019.

388

Figures and tables

391 **Figure 1** Representative example of individual and summed ground reaction force (GRF) profiles

392 reconstructed from the first five principal components (PCs), for a single trial of running at a constant

393 moderate speed. Individual principal GRFs (PGRFs; grey dotted lines) were added together as the

394 summed PGRFs (∑PGRFs; grey solid lines) for the first k PCs and compared to the measured GRF

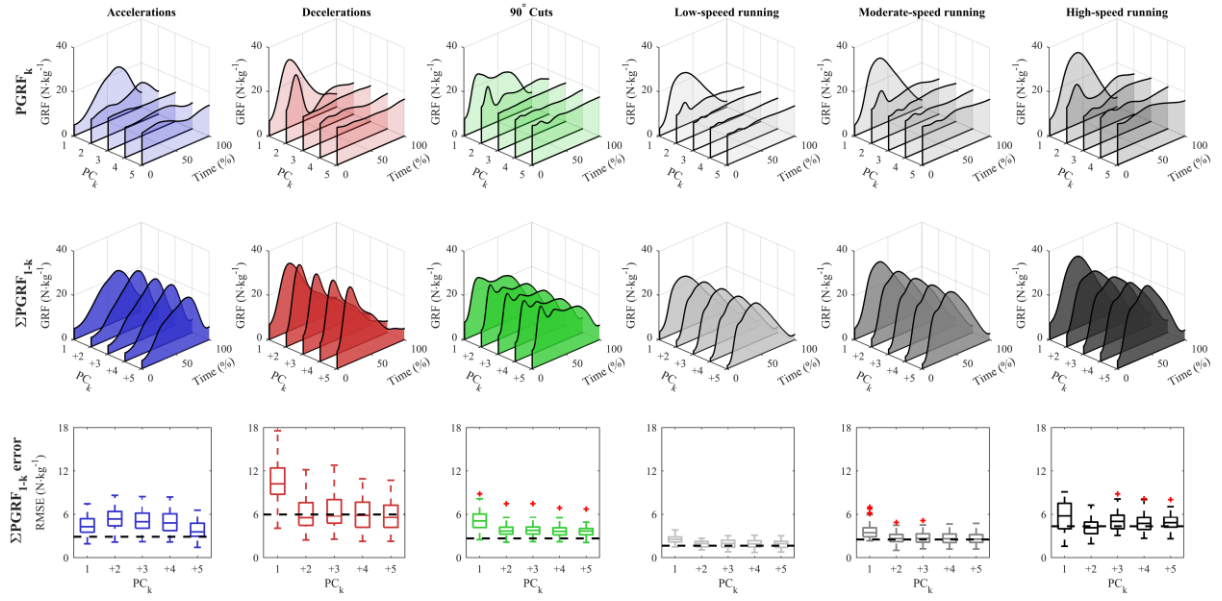395 (black solid line) by the curve root mean square error (RMSE).

396

Figure 2 Mean principal ground reaction forces (PGRFs) calculated from the first five principal components (PCs), for each task. PGRFs were calculated from principal accelerations (PAs) reconstructed from either the kth PC (top row), or the sum of the first k PCs ($\sum PGRF_{1-k}$; middle row). Root mean square errors (RMSE; bottom row) are mean errors for the $\sum PGRF$ profiles and the horizontal black line represents the RMSE for $\sum PGRFs$ from all 45 PCs (i.e. the original data).

Table 1 Principal components and ground reaction forces for the different tasks

	Principal components (k)					
	1	2	3	4	5	45
λ_k (%)	48.57	12.43	8.56	4.44	3.78	0
Cumulative λ (%)	48.57	60.99	69.55	73.99	77.77	100
	$\sum$PGRF RMSE (N·kg^{-1})					
Accelerations (n=80)	4.46 ±1.3	5.37 ±1.5	5.09 ±1.5	4.93 ±1.5	3.88 ±1.2	2.89 ±0.7
Decelerations (n=83)	10.69 ±3.1	6.18 ±2.3	6.44 ±2.4	6.11 ±2.2	5.88 ±2	5.97 ±1.8
90° Cuts (n=88)	5.11 ±1.3	3.77 ±0.9	3.79 ±0.9	3.65 ±0.8	3.61 ±0.7	2.66 ±0.7
Constant speed running						
Low (2-3 m·s^{-1}; n=81)	2.53 ±0.5	1.89 ±0.4	1.93 ±0.5	1.92 ±0.5	1.87 ±0.5	1.65 ±0.4
Moderate (4-5 m·s^{-1}; n=80)	3.74 ±1.1	2.70 ±0.8	2.82 ±0.9	2.72 ±0.8	2.66 ±0.7	2.51 ±0.6
High (>6 m·s^{-1}; n=71)	5.67 ±2	4.14 ±1.2	5.03 ±1.2	4.71 ±1.2	4.84 ±1.1	4.34 ±1.3
All tasks (n=483)	5.38 ±3.1	4.01 ±2	4.17 ±2.1	4.00 ±1.9	3.78 ±1.8	3.33 ±1.8

Summed principal ground reaction force ($\sum$PGRF) error results from the first k principal components (PCs), as well as all 45 PCs (i.e. original data). Eigenvalues λ_k represent the normalised amount of segmental acceleration variance explained by each PC$_k$. Root mean square errors (RMSE) are mean ± standard deviation values per PC$_k$ for each task.

403

404

20

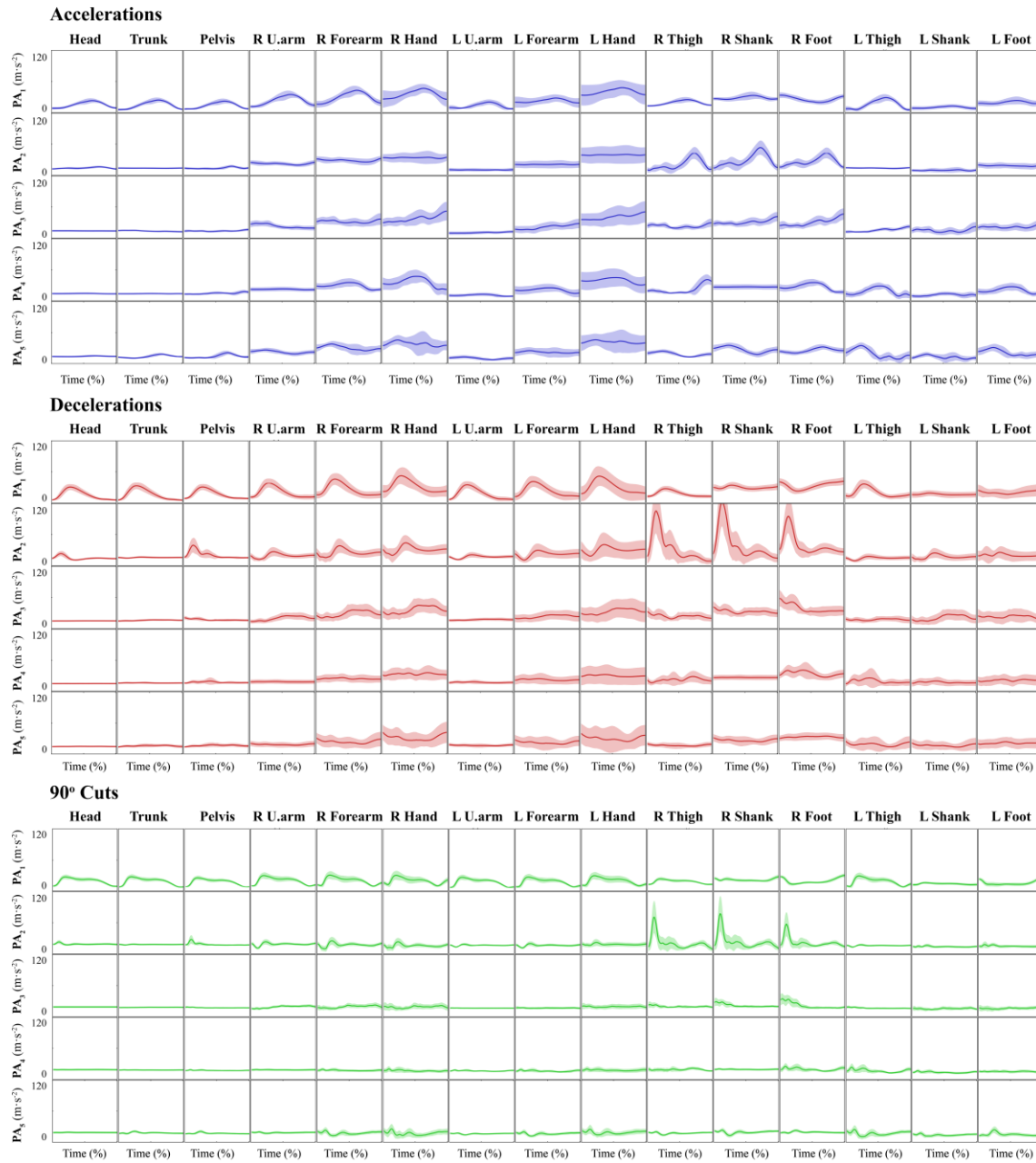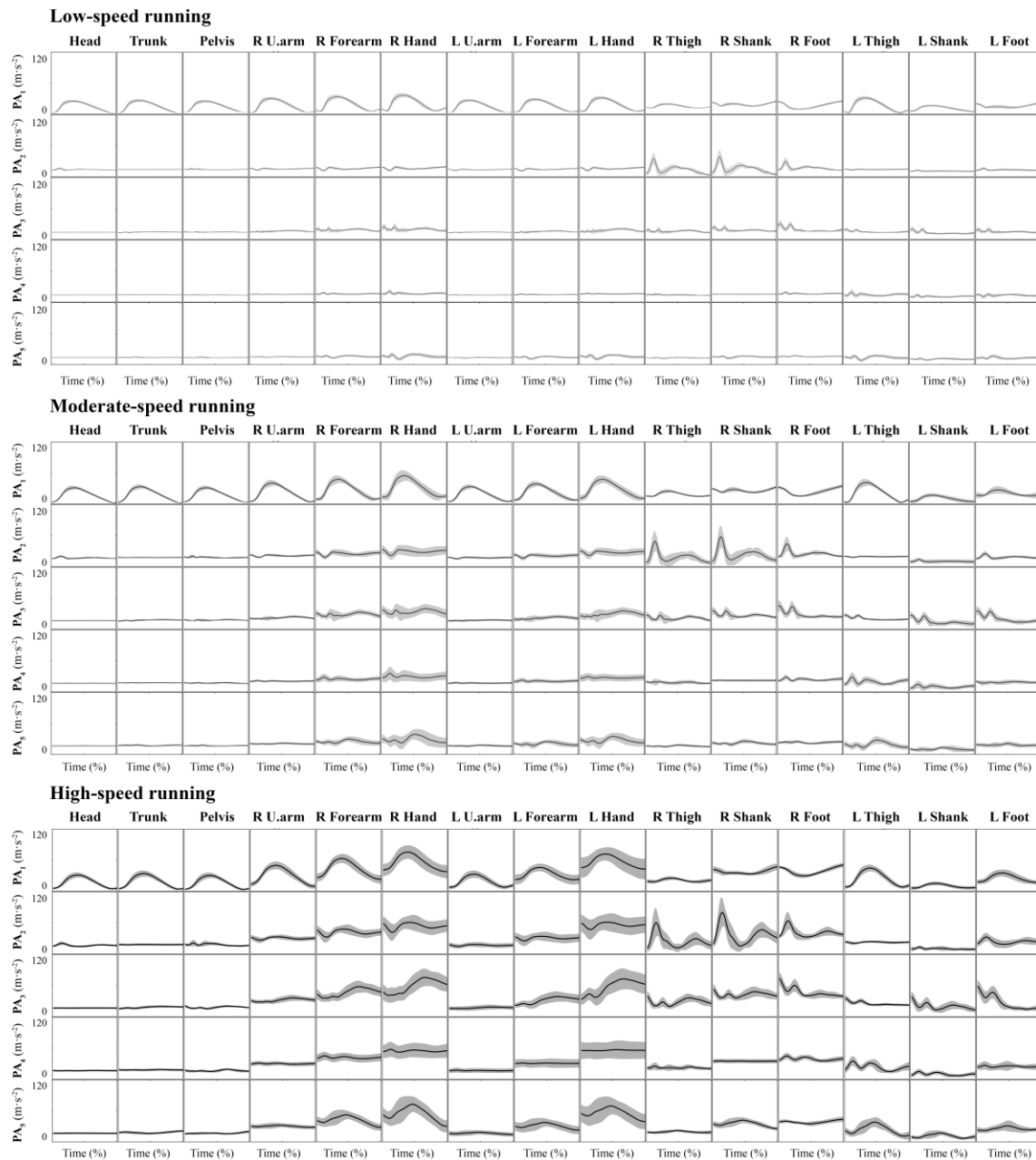**Appendix A: Principal segmental accelerations**

407   **Figure A.1** Principal accelerations (PAs) from the first five principal components (rows) for

408   accelerations (blue), decelerations (red) and 90° cuts (green) during a right leg contact phase. PA

409   profiles are mean ± standard deviation (shaded) curves from 0-100% of stance, for all fifteen segments

410   (columns).

411

412

413

Figure A.2 Principal accelerations (PAs) from the first five principal components (rows) for running

at constant low (light grey), moderate (grey) and high speeds (black) during a right leg contact phase.

PA profiles are mean ± standard deviation (shaded) curves from 0-100% of stance, for all fifteen

segments (columns).

418